Memoirs of the School of Engineering, Okayama University Vol.13, February 1979

Numerical Analysis of Oscillatory Combustion Phenomena generated in A Pipe-Type Combustor

Yutaka TANAKA *

(Received January 29, 1979)

Synopsis

In this paper, is proposed a calculating method for the simulation of oscillatory combustion state , and comparisons between estimation results and experimental ones are carried out. With respect to the effects of geometric dimensions of combustion system, and of fuel- and air-flow rate conditions on characteristics such as an amplitude of oscillation , its fluctuation , and a frequency, a theoretical analysis presents a correct estimation of the phenomena.

By use of this analysis, it becomes possible exactly to estimate the changes which take place in the combustion system. On the basis of the quantitative feature of the theoretical results, the influences of the factors such as ignition lag, wall temperature ratio, and heat transmission on the combustion oscillation are studied.

1. Introduction

Phenomena referred to as a general term of combustion instability are observed in almost all the types of continuous-flow combustors, and are classified into three types. The one is a succesive oscillation phenomenon of pressure, velocity, and others and is called by a name of oscillatory combustion. A second is a fluctuation behavior accompanied by abrupt changes of states and is termed an unstable combustion.

* Department of Mechanical Engineering

The remaining one is a fluctuation state which takes place in a pulsated manner and is named a pulsating combustion. Many workers have studied these non-steady combustion behaviors respectively from different points of view.

The above mentioned phenomena are always generated in a combustion chamber excepting the fluctuating behaviors of flame front termed flame front instabilities. Consequently, it should be considered that all the factors such as fuel- and air-pipe systems, geometries of chamber, flow rates, kind of fuel, and mixing ratio may take part in the oscillation phenomena. Because these complicated factors must be taken into consideration, only a few studies have been made about the generation of combustion instability and its foreknowledge. Needless to say, at present there are few studies which have been accomplished to a practical stage of application as a quantitative analyzing method.

However, on the other hand quantitative methods of analysis which employ the method of characteristic curve have been already established and have reached the practical stage for such phenomena as fluid oscillation, hydraulic transient, and water hammer in pipe systems [(1)-(4)] and the effects which arise from the velocity and pressure oscillations in the induction and exhaust systems [(5)-(7)] of internal combustion engines. By use of this method of characteristic curve it is easy to take geometries and effects of non-linear oscillation into consideration and it seems that such an analyzing method can be applied to the calculation about the phenomena which take place in the actual combustion chamber. In view of these concepts, if we adopt the numerical analyzing procedures which can introduce intensive heat release by combustion, heat transfer, diffusion of fuel component and others into analysis, it may also become possible quantitatively to treat the phenomena of combustion instability.

On the basis of these views, this report describes a numerical estimation method of those phenomena. Comparisons between experimental results and calculated ones are carried out concerning the self-excited oscillation in that combustion chamber for which the throttle resistance and the friction loss in induction pipes are exactly estimated, and which is hardly affected by the pressure fluctuation generated by an air compressor. This estimation is followed by an examination with respect to the effects of wall temperature, pipe friction, ignition lag, and of heat transfer between wall and flowing gas upon the oscillation phenomena.

2. Main notations

a : sound velocity

A : heat equivalence of work

A_s : sound velocity ratio

c_p, c_v : specific heat at constant pressure and specific heat at constant volume respectively

d : pipe diameter

D_k : diffusion coefficient [$= \lambda^{(e)}/(\rho\, g_c\, c_p\, L_e)$]

f : internal cross-sectional area of pipe

g_c : gravitational acceleration

h_f : calorific heat value of fuel

h_j : energy fluxes (j=1 : for heat release term, j=2 : for heat transfer flux term, j=3 : for heat conduction term, and j=4 : for energy term generated by friction between flowing gas and pipe wall)

l, L : lengths (l_{0s} : standard length)

L_e : Lewis number

p : pressure

Q_a, Q_f : air- and fuel-flow rates respectively

r : volume fraction (r_k : imaginary volume fraction of fuel component considering that the chemical species of burned gas are allowed to convert into original molecules of unburned state)

R : gas constant

R_e : Reynolds number

s_a : distance from burner port to the point of maximum heat release

S : entropy

t : time

T : absolute temperature (T : gas temperature, T_{0s} : ambient or reference temperature, T_w : wall temperature)

u : velocity

W : molecular weight

x : longitudinal distance along pipe axis

Y : mass fraction (Y_k : imaginary mass fraction of fuel component considering that the chemical species of burned gas are allowed to convert into the original molecules of unburned state)

α : heat transfer coefficient

Δ : minute amount of change

ζ : ratio of wall temperature rise to gas temperature rise [$= (T_w - T_{0s})/(T - T_{0s})$]

κ : specific heat ratio

$\lambda^{(e)}$: effective heat conductivity

Λ_p, Λ_e : wave lengths of pressure mode and of entropy mode respectively

ν : frequency

ξ : coefficient of pipe friction
ρ : density
σ : discharge coefficient
τ : elapsed time of gas travel after injection

[Subscripts]
k : for the state assuming that combustion doesn't take place (for imaginary values of unburned state converted from burned state)
0 : for values of state on the assumption that states are changed adiabatically to the surrounding state
$0s$: for the ambient or reference state
$+,-$: for downstream and upstream directions respectively under the definition that the positive direction of velocity u is toward the increased x
$-$: for time-averaged values used as a superscript

[Notations for systems] the following are written in bold face letters
P : pipe
T : throttle
V : reservoir

[Differential symbols]

$$D/Dt \equiv \partial/\partial t + u\partial/\partial x = (a_{0s}/l_{0s})(\partial/\partial Z + U\partial/\partial X) \equiv (a_{0s}/ l_{0s}) D/DZ$$
$$\Delta\pm/\Delta t \equiv \partial/\partial t + (u \pm a)\partial/\partial x = (a_{0s}/l_{0s})(\partial/\partial Z + (U \pm P A_s) \partial/\partial X)$$
$$\equiv (a_{0s}/l_{0s}) \Delta\pm/\Delta Z$$

where double signs indicate order type and the same is defined in the following.

[Fundamental expressions for the subscripts of 0 and $0s$, and non-dimensional variables]

$$a^2 = \kappa p/\rho \ , \ a_0^2 = p_{0s}/\rho_0 \ , \ \rho_0/\rho = (p_{0s}/ p)^{1/\kappa}$$
$$P = (p/ p_{0s})^{(\kappa-1)/2\kappa} , A_s = a_0/ a_{0s} , U = u/ a_{0s}$$
$$X = x/ l_{0s} , Z = t\, a_{0s}/ l_{0s} , F_\pm = U \pm 2 A_s P / (\kappa - 1)$$

3. Theoretical

The steady and non-steady combustion phenomena dealt with in the present paper are the changes and fluctuations of non-linear and one-dimensional types in the longitudinal direction. Therefore, all the

variables used are averaged over the cross-section of pipe. The fluctuations of pressure, velocity, composition of gases, temperature, and ignition lag are taken into consideration as driving factors of oscillation. Energy transfer fluxes are taken into account with a heat release term h_1, a heat transfer term h_2 between pipe wall and flowing gas, a heat conduction term h_3 between gases, and an energy generation term h_4 by the friction between gas and pipe wall. With respect to these energy transfer terms, experimental expressions are employed for calculating the coefficients of heat release term, heat transfer term, and of pipe friction term.

The following assumptions were set up for the development of the expressions; (1) Perfect gas law is applicable to the change of state of gas, (2) For the simplification of the conservation law of chemical species, the concentration Y_k and r_k are considered to be the mass and volume fractions of fuel component when the chemical species obtained by gas analysis of combustion products are converted to the molecular components in original unburned state. The fuel fraction for pilot flame is involved in this imaginary fraction of concentration. (3) The wall temperature for oscillation period varies with location but not with time. (4) Physical values such as L_e, $\lambda^{(e)}$, c_p, c_v, R remain constant independently of both position and time.

The fundamental expressions used in conformity with the above-mentioned views are:

perfect gas law :

$$p = \rho g_c R T \quad \cdots\cdots(1)$$

mass concentration law :

$$D\rho / Dt + \rho \partial u / \partial x = 0 \quad \cdots\cdots(2)$$

momentum conservation law :

$$Du / Dt + (1 / \rho) \partial p / \partial x + (\xi / d) u |u| / 2 - g_c = 0 \quad \cdots(3)$$

energy conservation law :

$$DS / Dt = \sum_{j=1}^{4} h_j / (T \rho g_c f) \quad \cdots\cdots(4)$$

and chemical species conservation law :

$$\rho Y_k D \ln Y_k / Dt - \partial / \partial x (\rho D_k \partial Y_k / \partial x) = 0 \quad \cdots\cdots(5)$$

3.1 Energy transfer terms

Longitudinal distance from burner port is taken as x, and final combustion efficiency of fuel is expressed as $\varepsilon_{ulti}(Y_k)$ as a function of imaginary mass fraction Y_k. The heat release rate in steady combustion state, that is, in time-averaged state, per unit time and per unit

length is expressed as ;

$$\overline{h}_1(x) = \overline{\rho}\, g_c\, \overline{u}\, f\, \overline{Y}_k\, \overline{\varepsilon}_{ulti}(\overline{Y}_k)\, h_f\, \eta_x(x) \quad \cdots\cdots(6)$$

The heat release rate $\eta_x(x)$ is experimentally expressed as a function of s_a in the following equation [8),(12)],

$$\eta_x(x) = (x / \overline{s}_a^{\,2}) \exp(- x / \overline{s}_a) \quad \cdots\cdots(7)$$

The expression of heat release distribution in the non-steady combustion state has to be set up in such a way that the expression may be also applicable to the oscillating case of each density, concentration, combustion efficiency, and heat release rate. On the basis of Eqs.(6) and (7), it is expressed as :

$$h_1(x, t ; \tau) = \rho\, g_c\, f\, Y_k\, \varepsilon_{ulti}(Y_k)\, h_f\, \eta(x, \tau) \quad \cdots\cdots(8)$$

In order that $\eta(x,\tau)$ implies the meanings of the product of u and $\eta_x(x)$ in the steady state, $\eta(x,\tau)$ is expressed as ;

$$\eta(x, \tau) = C_2(x) \frac{\tau}{\tau_{ign}^{\,2}} \exp(- c_1(x)\, \tau / \tau_{ign}) \quad \cdots\cdots(9)$$

where, τ_{ign} is the average time required for the reactants to travel the distance from the injection point of x= 0 to the point of x=x, and is termed ignition lag. The symbols τ, τ_{ign}, $c_1(x)$, and $c_2(x)$ are defined as follows;

$$\left.\begin{aligned} \tau &= \frac{x}{\int_0^x u\, dx / x}\ , \quad \tau_{ign} = \frac{\overline{s}_a}{\int_0^{\overline{s}_a} \overline{u}\, dx / \overline{s}_a}\ , \quad c_1(x) = \frac{\int_0^x \overline{u}\, dx / x}{\int_0^x \overline{u}\, dx / \overline{s}_a}\ , \\ c_2(x) &= c_1(x) \frac{\overline{u}}{\int_0^{\overline{s}_a} \overline{u}\, dx / \overline{s}_a} \end{aligned}\right\} \quad (10)$$

These are determined by use of time-averaged combustion fields, and the non-steady heat distributions are estimated by introducing these values into Eqs.(8) and (9).

By heat transfer, heat flux h_2 is transmitted from pipe wall to internal gas at the temperature T, then h_2 is evaluated from

$$h_2 = \alpha\, \pi\, d\, (\overline{T}_w - T) \quad \cdots\cdots(11)$$

where heat transfer rate α is estimated by reference (9) such that

$$\alpha = C_T\, (\rho\, g_c\, u)^{0.8} / d^{0.2}\ , \quad C_T = 3.095 \times 10^{-4} \quad \cdots\cdots(12)$$

By heat conduction, heat flux h_3 is conducted from higher temperature gases to lower temperature gases, then h_3 is evaluated from,

$$h_3 = f\,\partial / \partial x \,(\lambda^{(e)} \,\partial T / \partial x) \quad \cdots\cdots\cdots\cdots\cdots\cdots (13)$$

Heat flux h_4 imparted to the gas owing to the convertion of friction energy becomes

$$h_4 = \rho\, u\, f\, A\, \xi\, u\, |u| \;/\; (2\, d) \quad \cdots\cdots\cdots\cdots\cdots\cdots (14)$$

where, by use of Blasius equation [10], ξ is expressed as a function of R_e in such a way that:
for turbulent flow;

$$\xi = 0.3164\, R_e^{-0.45}$$

in case that ξ is greater than 0.08 in the above equation;

$$\xi = 0.08 \qquad \cdots\cdots (15)$$

4. Arrangement of fundamental equations

4.1 Characteristic equations

By arranging the equations mentioned in the preceding chapter on the basis of the assumptions in chapter 3 and of the non-dimensional notations in chapter 2, the following types of differential equations are derived with respect to the changes of state which follow the respective characteristic curves of pressure and entropy modes.

(a) The change along the characteristic curve

$$\delta X / \delta Z = U \quad \cdots\cdots\cdots\cdots\cdots\cdots (16)$$

of entropy mode becomes with regards to A_s as follows;

$$\frac{1}{A_s}\frac{D\,A_s}{D\,Z} = \frac{\kappa - 1}{2\,\kappa}\,\frac{1}{f\,A}\,\frac{l_{0s}}{a_{0s}\,p_{0s}}\,P^{-2\kappa/(\kappa-1)}\sum_{j=1}^{4} h_j \quad \cdots\cdots\cdots\cdots (17)$$

and the imaginary fuel fraction Y_k changes according to the equation of

$$\frac{D\,Y_k}{D\,Z} = D_{k.0s}\,\frac{1}{l_{0s}\,a_{0s}}\,\frac{A_s^2}{P^{2/(\kappa-1)}}\,\frac{\partial^2 Y_k}{\partial\, X^2} \quad \cdots\cdots\cdots\cdots\cdots\cdots (18)$$

The symbol Y_k is related to r_k by the equation of

$$Y_k = W_k\, r_k \;/\; (\sum_i W_i\, r_i) \quad \cdots\cdots\cdots\cdots\cdots\cdots (19)$$

but the molecular weight of mixture is regarded as being constant throughout combustion period, then r_k is considered to be expressed in a similar type equation to Eq.(18).

(b) The change along the characteristic curve of

$$\delta_{\pm} X / \delta Z = U \pm A_s P \quad \cdots\cdots(20)$$

is expressed as

$$\frac{\Delta_{\pm} F}{\Delta Z} \equiv \frac{\Delta_{\pm} U}{\Delta Z} \pm \frac{2}{\kappa - 1} \frac{\Delta_{\pm} (A_s P)}{\Delta Z}$$

$$= \pm \frac{2}{\kappa - 1} P \frac{\Delta_{\pm} A_s}{\Delta Z} \pm \frac{\kappa - 1}{f A} \frac{l_{0s} A_s}{\rho_{0s} a_{0s}^3 P^{(\kappa+1)/(\kappa-1)}} \sum_{j=1}^{4} h_j$$

$$+ \frac{l_{0s}}{a_{0s}^2} g_c - \frac{\xi}{d} l_{0s} \frac{u |u|}{2}$$

$$\cdots\cdots(21)$$

where, duplicate signs and duplicate subscripts mean order types respectively.

4.2 Equations for boundary conditions

Flow rate, chemical species flow rate, momentum, and energy which pass through reservoir, pipe, and throttle, are respectively expressed as;

Flow rate :

$$\rho f u = \rho_{0s} a_{0s} f P^{2/(\kappa - 1)} U / A_s^2$$

Chemical species flow rate :

$$\rho f u Y_k = \rho_{0s} a_{0s} f Y_k P^{2/(\kappa - 1)} U / A_s^2$$

Momentum flux :

$$\frac{\kappa}{\kappa - 1} \frac{P}{\rho} + \frac{u^2}{2} = \frac{a_{0s}^2}{\kappa - 1} \left(P^2 A_s^2 + \frac{\kappa - 1}{2} U^2 \right) \qquad (22)$$

Energy flux :

$$\left(\frac{\kappa}{\kappa - 1} \frac{P}{\rho} + \frac{u^2}{2} \right) \rho f u = \frac{\rho_{0s} a_{0s}^3}{\kappa - 1} f \left(P^2 A_s^2 + \frac{\kappa - 1}{2} U^2 \right) \cdot$$

$$\cdot P^{2/(\kappa - 1)} U / A_s^2$$

Because it is difficult to derive a solution which simultaneously satisfies the above four boundary equations, the following assumptions

and judgements are used in order to simplify those equations : (1) The velocity in the reservoir is zero. (2) When gases enter the larger pipe or the reservoir from the smaller pipe or through the throttle, the pressure at the outlet section of the smaller pipe or of the throttle becomes equal to the pressure at the inlet section of the larger pipe or of the reservoir. (3) When the gas enters the smaller pipe or the throttle from the larger pipe or the reservoir, the gas undergoes an adiabatic change. (4) Vena contracta arises when gases pass through the throttle, and hence the apparent throttle area becomes equal to the product of a discharge coefficient σ and a throttle area f. (5) Each pressure at the branched sections at which three pipe ends are combined becomes equal to the averaged value among them. (6) Once the fuel effuses out of the combustion chamber, its calorific value becomes zero. The pressure at the section just out of the combustion chamber is equal to the atmospheric pressure, but the temperature of the fluid at that section is determined from the consideration that the fluid undergoes an adiabatic change from the chamber pressure to the atmospheric pressure.

In order to shorten the time required for calculation, the following judgements are made. (7) The fluid at the boundary flows from the higher side of the imaginary shut-off pressure to the lower side of the imaginary shut-off pressure, which is expressed as $P + (\kappa - 1)U/(2A_s)$ at the left side of the boundary or $P - (\kappa - 1)U/(2A_s)$ at the right side of the boundary if the plus direction of u is directed from left to right. Similarly at the branched section it can be said that the pipe, in which the pressure higher than that obtained by the above-mentioned assumption (5) occurs is a discharge pipe and that the pipe in which a lower pressure occurs is an inflow pipe.

The following correction is made in order to eliminate the errors apperaing in A_s at the inflow section, which are attributable to the numerical calculation procedure that the pipes are divided into finite length pieces. (8) The magnitudes of A_s, Y_k, and r_k at inflow section are determined from the inflow and discharge balances both of mass flux and of energy flux within the time increment of ΔZ on the assumption that the fluxes flow in and are discharged from the control volume which is equal to the product of the length of divided piece ΔX and the cross-sectional area f.

5. Numerical procedures

5.1 Frequency range which the method of characteristic curve can express

and the analyzing method for the change in pipe systems

Characteristic velocity of pressure mode $|u \pm a|$ and that of entropy mode $|u|$ are related to the frequency ν, and to the wave length Λ by the following expression.

$$|u \pm a| = \nu \Lambda_p, \quad |u| = \nu \Lambda_e \quad \ldots\ldots (23)$$

By the use of the equation (23) and of the fact that the minimum wave lengths Λ_p for pressure mode and Λ_e for entropy mode which can be expressed by the method of characteristic curve are equal to twice their respective divided lengths for calculation Δx_p and Δx_e, the numerical procedure can express the fluctuation in the frequency range of

$$0 \leqq \nu < min[|u \pm a|/(2\Delta x_p), |u|/(2\Delta x_e)] \quad \ldots\ldots\ldots\ldots (24)$$

Since the sound speed a is much faster than the gas speed u, it is desirable in order to obtain an exact solution of both modes that the ratio of Δx_e to Δx_p be represented in the following relation ;

$$\Delta x_e / \Delta x_p = |u| / |u \pm a| \quad .. (25)$$

Figure 1 indicates the successive calculating procedure of the pressure mode components P and U and of the entropy mode components r_k, T, etc. The components of both modes at the time $Z = Z$ are regarded to have been already obtained for the grids points placed at the respective non-

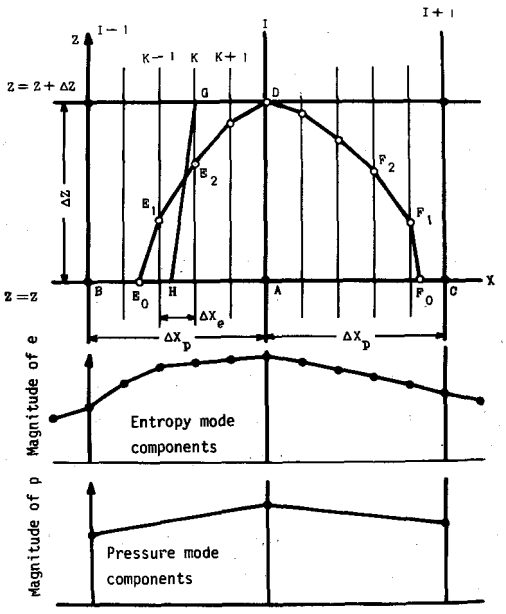

Fig.1 Characteristic grids and characteristic curves

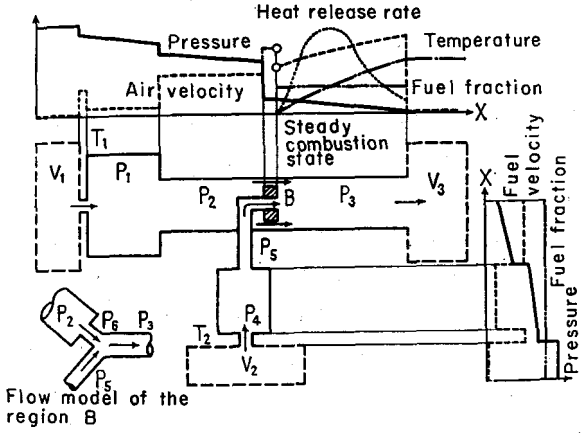

V Reservoir
1 Air
2 Fuel
3 Surroundings

P Pipe
1 Air plenum chamber
2 Air supplying pipe
3 Combustion pipe
4 Fuel plenum chamber
5 Fuel supplying pipe
6 Throttle pipe

T Throttle
B Flame holder

Fig.2 Terms of combustion systems and steady combustion states

dimensional grid spacings ΔX_p and ΔX_e as shown in the lower parts of the figure. Where, the known values are plotted by solid circles under the coordinate system with x taken as abscissa against $p(I)$ and $e(I)$ as ordinate. The entropy mode value at a point H which will hereinafter be used in description can be obtained by interpolation between the magnitude of $e(K-1)$ and that of $e(K)$. Similarly, the pressure mode values at the points E_0 and F_0 can be respectively obtained by the interpolations between the magnitudes of $p(I-1)$ and $p(I)$, and between those of $p(I)$ and $p(I+1)$. The value at the time $Z = Z + \Delta Z$ is determined according to the upper part of the same figure. For instance, the entropy mode value at the point G is calculated by the use of the value at the point H, the direction from H to G, and of the equations from (16) to (19) which express the change between the points of H and G. The time τ required for the gas to travel up to the point G is equal to the sum of the gas travelling time up to the point H and the time $l_{0s}\Delta Z/a_{0s}$. The pressure mode values of non-dimensional variables F_+ and F_- at the point D are determined both by the calculation of the change of Eq.(21) along the characteristic curve of Eq.(20) and by the use of the respective variables F_+ and F_- at the points E_0 and F_0. Then, the points E_0 and F_0 are decided as the cross-points where the abscissa $Z = Z$ intersects with the upstream and downstream directed characteristic curves which ultimately pass through the point D.

Tab.1 Fundamental constants

Notation	Value	Unit	Expression
Ambient temp.	300	°K	
Ambient press.	1.0	kg/cm^2	
Fuel used	C_3H_8		
Calorific value	8000.0	kcal/(kg.fuel)	
Specific heat at const. pressure	0.24	kcal/(kg.°K)	
Specific heat ratio	1.4		
Effective viscosity	0.16	cm^2/s	μ/ρ
Effective conductivity	10^{-4}	kcal/(cm.s.°K)	$\lambda^{(e)}$
Pipe friction	0.3164		Coef. of Eq.(15) of ξ
Heat transfer	3.095×10^{-4}		Coef. of Eq.(12) of C_T
Wall temp. ratio	0.8		ζ
Ignition lag	0.02	s	

Pipe length		Symbols of meas. points	Distance from pipe entrance
P_1	88.0 cm	b	80.0 cm
P_2	50.4 cm	a	31.0 cm
P_3	200.0 cm	d	133.0 cm
P_4	40.0 cm	c	8.0 cm
P_5	42.3 cm		

Pipe diameter		
P_1	55.4 cm	
P_2	8.07 cm	Discharge coeff. σ at outlet
P_3	8.07 cm	σ_{out}=1.0 for discharge
		σ_{in} =0.9 for flow in
P_4	4.00 cm	
P_5	0.80 cm	
P_6	7.01 cm	

Throttle diameters		Discharge coefficients σ
T_1	1.8 cm	1.0
T_2	0.2 cm	1.0

Fuel for pilot flame	134.0 cc/s

5.2 Calculation procedures

Combustion chamber is modelled in the parts of reservoir, throttle, pipe, and branch as illustrated in Fig.2. Where, the air and fuel supplying pipe systems and the surrounding atmosphere are taken as reservoirs and the air- and fuel-plenum chambers are taken as pipes. Lower parts of Tab.1 show the dimensions of combustion chamber,and the measuring and calculating points. Upper parts of the same table represent the fundamental constants. Among those constants, $\lambda^{(e)}$, ζ and τ_{ign} were derived from the time-averaged combustion state measured under the flow rate condition of the air flow rate Q_a = 15.7 10^3 cc/s, of the fuel flow rate Q_f = 243 cc/s, and of the fuel flow rate for pilot flame of 134 cc/s, and under the dimensional conditions of above-mentioned main part dimensions of combustion systems.In order to simplify the problems, those fundamental constants are always used, except when they are used as a variable or a parameter.

According to the flow chart illustrated in Fig.3, the calculation was executed in the following way; (1) By the use of the equations of time-averaged types mentioned in chapters 3 and 4, steady state distributions are determined [8] for pressure, velocity, heat release rate, concentration, temperature, travel time of gas after injection from burner port, and other necessary values. (2) Resonance frequency is estimated on the assumption that the pipe systems act as a Helmholtz resonator. The pipe P_1 is regarded as the reservoir of volume V_{P1} and the pipes of P_2 and P_3 are regarded as one pipe whose length and cross-sectional area are equal respectively $L_{P2}+L_{P3}$ and f_{P3}, thereby the resonance frequency ν_H is estimated by

$$\nu_H = \frac{a_{0s}}{2\pi}\sqrt{f_{p3} / [(L_{p2} + L_{p3}) V_{p1}]} \quad \cdots\cdots\cdots\cdots (26)$$

(3) The steady state distributions obtained in (1) are taken as initial values for calculation, then the internal state of each pipe is successively solved by the use of the equations of character-

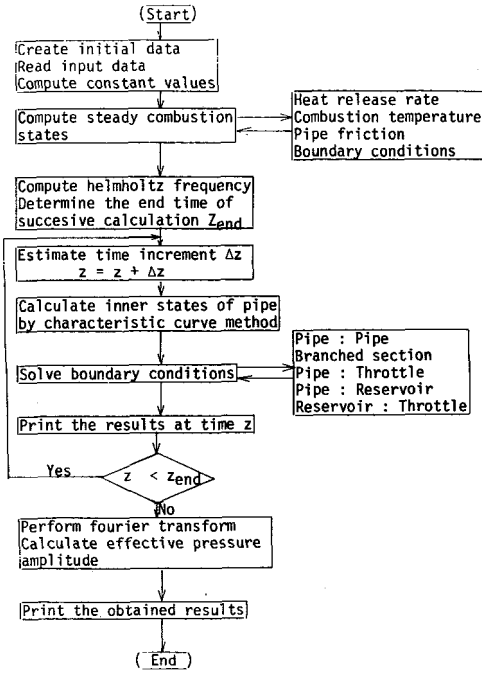

Fig.3 Flow chart of calculation

istic curves and of boundary conditions. (4) With respect to the pressure changes successively obtained in (3), the first Fourier transformation is carried out within the time interval from zero to $1/\nu_H$. If the transform coefficients of sine and cosine types are respectively designated by $P_{Fsin.j}$ and $P_{Fcos.j}$, where j stands for integers varied from first to $jend$-th, the effective value of pressure amplitude P_m is calculated from the following equation,

$$P_m = \sqrt{\sum_{j=1}^{jend} \left[\left(p_{F.sin.j} \right)^2 + \left(p_{f.cos.j} \right)^2 \right]} \qquad \text{.....(27)}$$

(5) Runs of Fourier transform are repeated by successively shifting its starting time. Similarly to the case of the actual self-excited oscillatory combustion, the effective amplitude of oscillation obtained theoretically also varies with time in such a way that its periodic time may be on the order of maximally several times the Helmholtz periodic time. In comparison of variation feature of amplitudes appearing in both experimental and theoretical wave forms, presented in this paper are the ones evaluated within a limited period equal to 5 times as long as Helmholtz periodic time.

Although numerical calculation presents separate results only for a particular condition of time-mean flow rate, experimant can give continuous results over a long period. Therefore, in a large portion of this paper, calculated results are depicted by plot points and experimental ones drawn in curves.

6. Results and discussions

Firstly, we explanate what and how are the feature of oscillatory combustion encountered in our experimental measurements by use of the data illustrated from Fig.4 to Fig.7.

Figure 4 shows the time-course of the effective pressure amplitude observed when air flow rate is gradually increased within the periods ranging from ignition to flame blow off. This figure states that not only pressure fluctuation but also its variation varies both for the changes of flow rate and of time-elapse, and it is seen that the features of effective pressure amplitude are classified into three patterns: the one lies in a low air flow rate region from point A to point B, points that are designated in the same figure, and shows low pressure amplitude but relatively high pressure amplitude variation; the second lies in a region from point B where the pressure fluctuation increases steeply to some point C, between which its pressure amplitude becomes

the highest but its variation is relatively low; and the last lies in flow rate region within point C and point D at which flame was blown off and shows the middle level of pressure amplitude but large amplitude variation.

Figure 5 indicates the pressure wave forms at three measuring point, which was already shown in Table 1. Wherein, the abscissa is regarded in the measure of 1sec/9div. From Fig.5a to Fig.5c, the figures are aligned in series from lower flow rate to higher ones. Especially between them, Fig.5b indicates the pressure wave forms just when the obvious oscillatory combustion begins.

In this manner, patterns of pressure oscillatory vary both with time and with flow rate; thus the observed pressure oscillation seems to be composed of the wave forms that higher order ones are superimposed over the pressure wave of about 7 Hz Helmholtz frequency. In addition, the wave form showed a beat type feature and the periodic time of this time-change of amplitude became 2/3 sec for the low air flow rate of Q_a = 11.5×10^3 cc/s of Fig.5a and became 1/7 sec to 1/4 sec for the higher flow rate condition of Fig.5c.

Fig.6 shows frequency spectrums of pressure fluctuation. Spectrum of Fig.6a are arranged for the change of air flow rate and that of Fig.6b are arranged for the change of volume of air reservoir (plenum chamber). Each spectrum has many amplitude peaks for frequency change. In these figures it is clearly shown that the magnitude of peaks and the frequency at the peaks vary with the volume of air plenum chamber and with the air flow rate. The broad peak about ten Hz is a helmholtz resonance frequency and the sharp peaks over about one hundred Hz are fluctuations generated by oscillatory heat release, and the latter ones

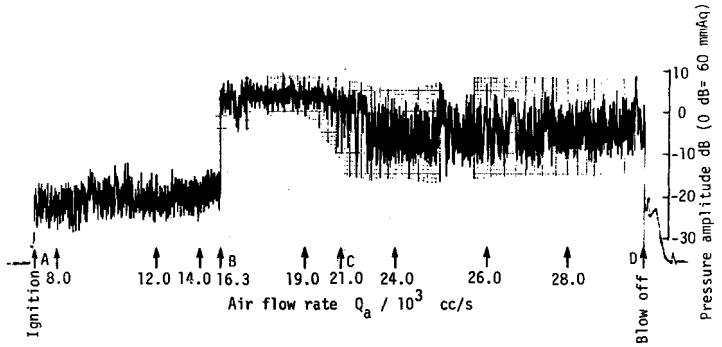

Volume of air plenum chamber 225×10^3 cc, Length of combustion pipe 200 cm
Fuel flow rate 243 cc/s, Measuring point a

Fig.4 Time-course of an effective pressure amplitude

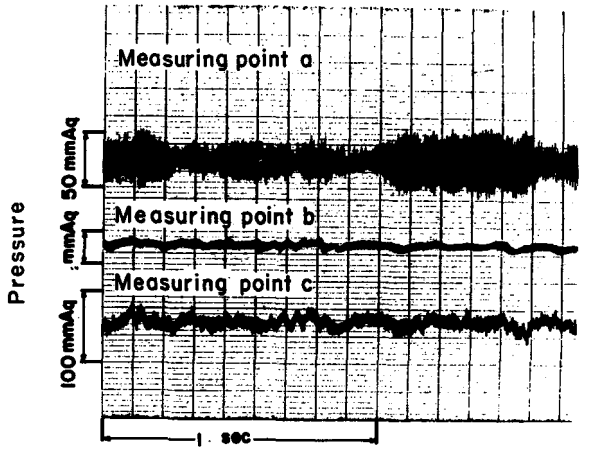

Volume of air plenum chamber 225×10^3 cc, Length of combustion pipe 200 cm
Air flow rate 11.5×10^3 cc/s, Fuel flow rate 243 cc/s

a : at low air-flow rate

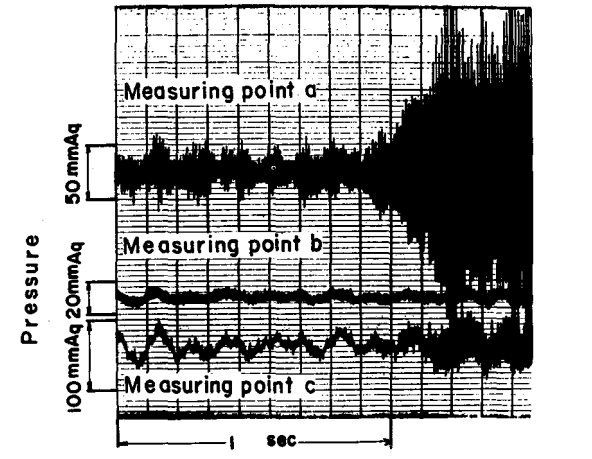

Volume of air plenum chamber 225×10^3 cc, Length of combustion pipe 200 cm
Air flow rate $(16.0 \sim 46.5) \times 10^3$ cc/s, Fuel flow rate 243 cc/s

b : at middle air-flow rate and at the initiation of oscillatory combustion

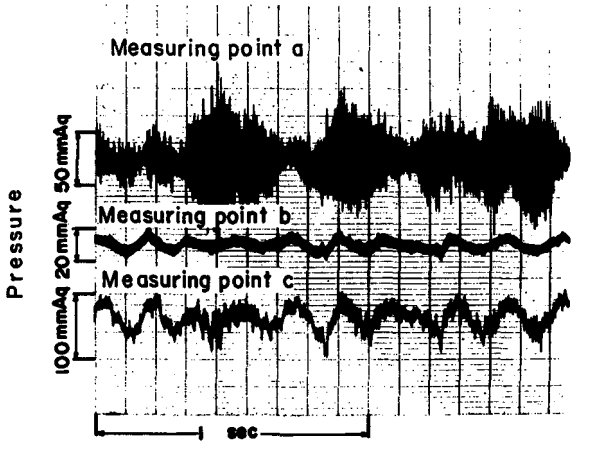

Volume of air plenum chamber 225×10^3 cc, Length of combustion pipe 200 cm
Air flow rate 16.5×10^3 cc/s, Fuel flow rate 243 cc/s

c : at high air-flow rate

Fig.5 Pressure wave - forms for three flow rate conditions

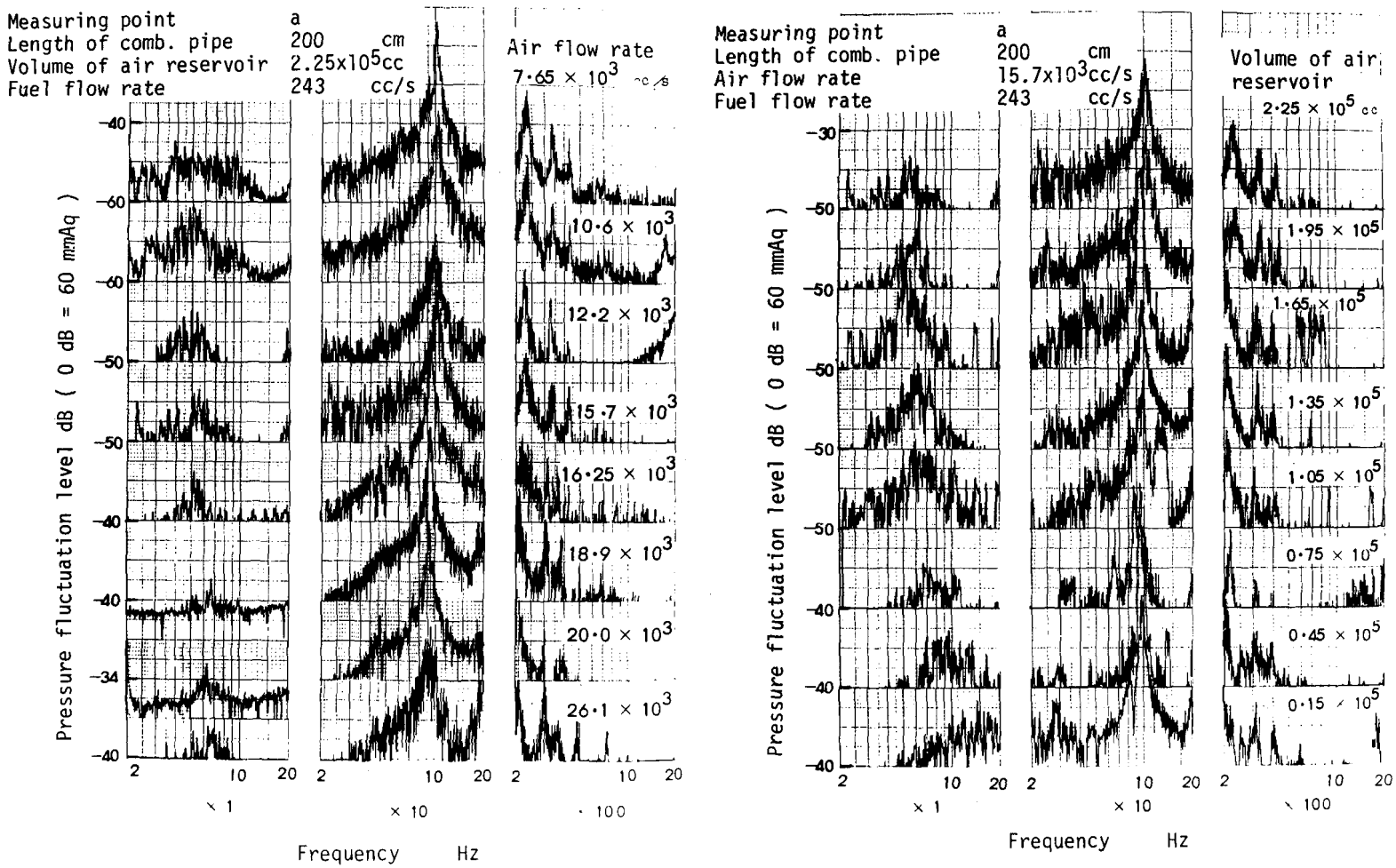

Fig.6 Frequency spectrums of pressure fluctuations

play the principal part of the observed pressure amplitude.

Figure 7 represents a three-dimensional picture of the relation among air flow rate, fuel flow rate, and effective pressure amplitude. Solid curves indicate the maximum and minimum pressure amplitudes when the fuel flow rate is kept constant, but that the air flow rate is variable. Blow off limit curve is also drawn in this figure. Together with Fig.4, it seems that this limit doesn't correspond with the points where the pressure amplitude becomes maximum or with the points where the pressure amplitude will steeply rise with an increase in air flow rate, that is, the beginning points of oscillatory combustion; but it lies in a low range of pressure amplitudes.

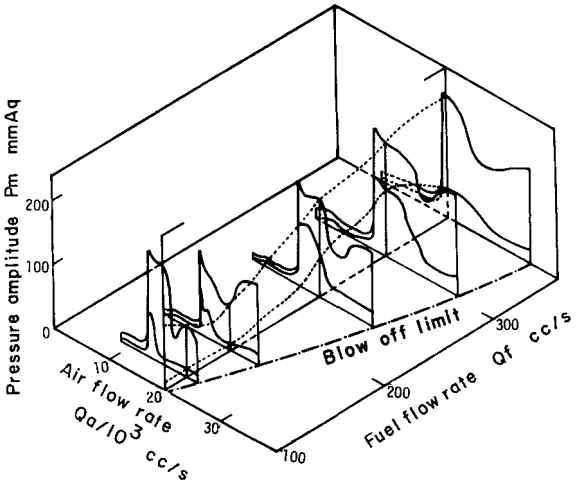

Fig.7 Variations of pressure amplitude with flow rate

Figure 8 illustrates the theoretically obtained fluctuating views of the distributions at regular time intervals of one-16th of Helmholtz periodic time of pressure, velocity, temperature volumetric fraction of concentration,

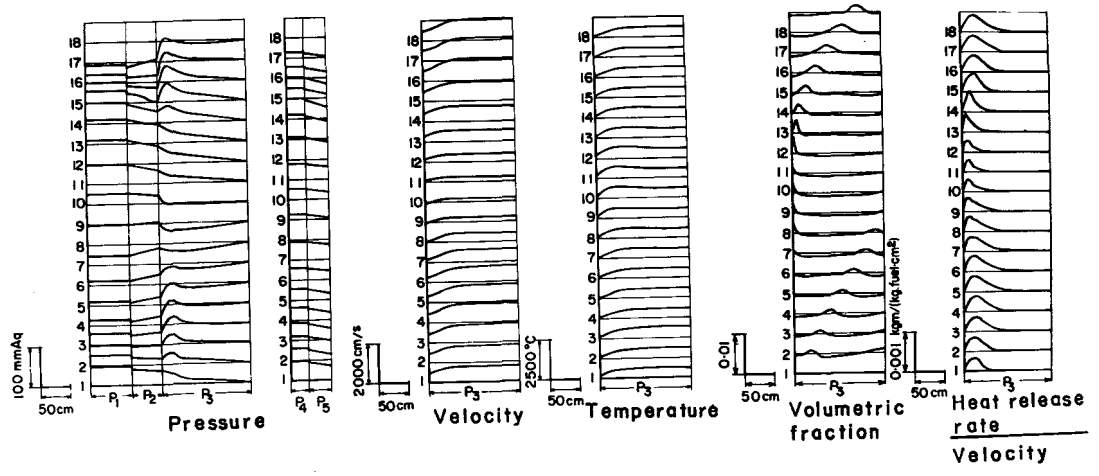

Fig.8 Fluctuating states in the combustion system

and that ratio of heat release rate to velocity, which precisely indicates the ratio of heat release per unit time and per unit length to the local velocity at the same place.

The flame holder is placed at the boundary between P_2 and P_3, and the pressure in P_3 changes largely near this holder. The cause of this change lies in that the concentration waves are formed and flow downstream, thereby generating waves of heat release rate, and that the waves act as a source exciting the pressure variations.

When a periodically oscillated flow rate of steady amplitude was in the non-combustion state given to the pipe system, amplitude variation of pressure wave scarcely occurred in every place of pipe systems. On the contrary, in the combustion state [11] the amplitude variation has been observed. Considering these facts with the results obtained in the present paper, it may be said that such an amplitude variation is caused by the interference effects between pressure mode and entropy mode variations.

Figure 9 shows the frequency spectrum of pressure wave evaluated at the point C, and the upper and lower figures respectively indicate

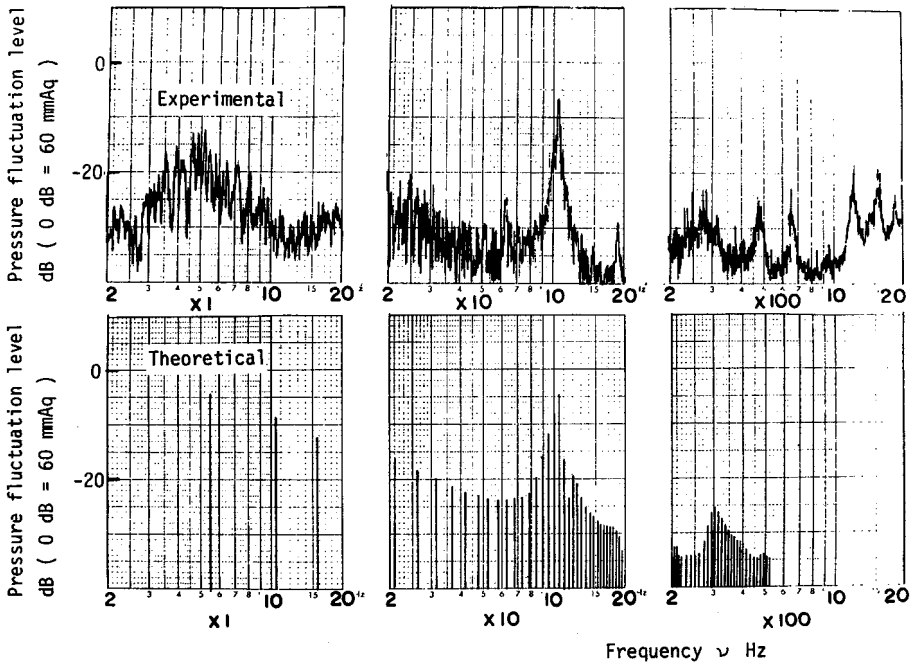

Volume of air plenum chamber 225×10^3 cc, Length of combustion pipe 200 cm
Air flow rate 20.6×10^3 cc/s, Fuel flow rate 243 cc/s
Measuring point c

Fig.9 Comparisons between experimental and theoretical spectrums

experimental and theoretical spectrums. The theoretical one is the analyzed result within one helmholtz periodic time and it agrees fairly well with the experimental one.

Figure 10 represents the pressure amplitude and the frequency change except for the Helmholtz frequency as the length of combustion pipe P_3 is varied. The numbers indicated in the frequency figure are given in such a way that the Helmholtz frequency may be taken as first order, then the frequencies of oscillation clearly perceived are numbered in ascending order of magnitude. Measured values are indicated by solid lines which connect triangle plots and calculated values are plotted by open circles. The first order frequency is not written in the figure, since it remains nearly constant against the change of pipe length, but seeing the higher order ones, it is recognized that the frequencies from second to fourth order increase with a decreasing pipe length. On the contrary, it can be seen that the pressure amplitude increases in proportion to an increase in pipe length. In every case the theoretical results agree well with the experimental ones.

Figure 11 shows the dependence of the clearly perceived frequencies on the volume of air plenum chamber when its volume is altered by

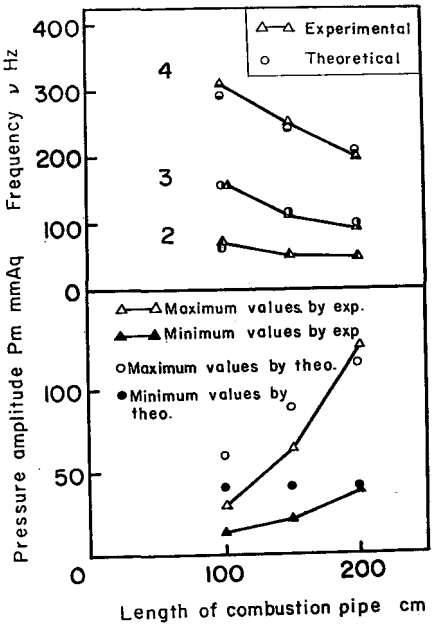

Fig.10 Relations among the length of combustion pipe, pressure amplitude, and its frequency

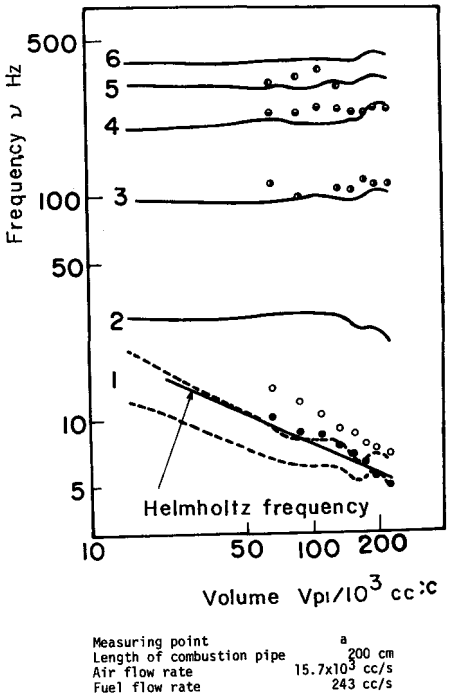

Fig.11 Changes of the clearly perceived frequencies with the volume of air plenum chamber

shortening the pipe length. With respect to the first order component ; (1) Since the pressure peak in the chart of the measured frequency spectrum is broadened, the first order component which represents the frequency range at the pressure 3 dB lower than the peak pressure is drawn by two broken curves. (2) In the theoretical treatment, at first wave forms as indicated in Figs.(4) and (5) are drawn, and next, five couples of each interval between peaks and between nodes are measured , finally, the highest frequency and the lowest frequency among those couples are respectively plotted by open circles and solid circles,and (3) the values estimated by Eq.(26) are drawn by solid curves.

Figure 12 shows the changes of pressure amplitude with the volume of the air plenum chamber. In both Figures 11 and 12, the theoretical values are in fairly good agreement with the experimental values for large volumes, but discrepancies between those values are somewhat increased with a decreasing volume. This is because, the volume diminished by the reduction of the pipe length, hence, the ratio of pipe diameter to pipe length became greater, and consequently, the change in state of flowing gas deviated from the one-dimensional assumption. Such errors should be minimized by analyzing P_1 as a reservoir.

Figure 13 shows the changes of pressure amplitude with air flow rate. In a wide range of air flow rates Q_a ranging from 15×10^3 cc/s to 25×10^3 cc/s, the theoretically obtained amplitudes fairly predict the experimentally obtained behaviors including an abrupt pressure

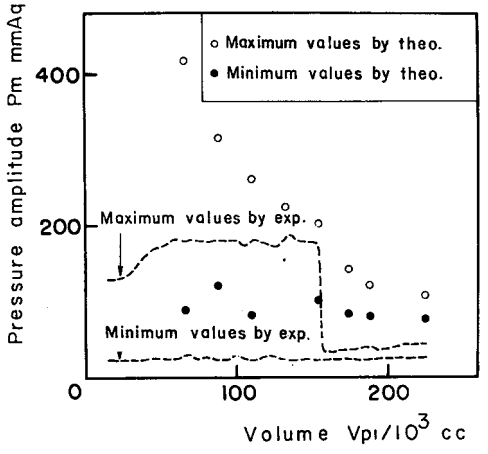

Fig.12 Changes of pressure amplitude with the volume of plenum chamber

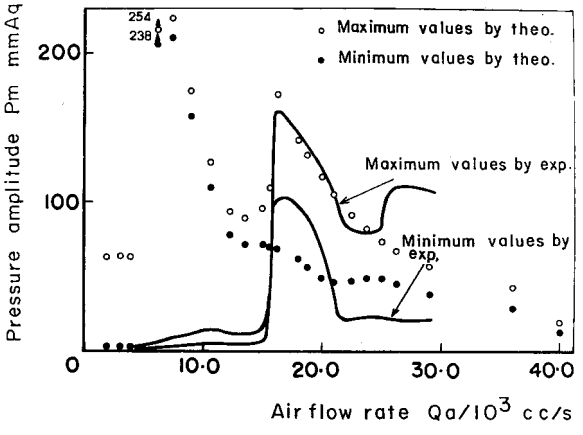

Fig.13 Relations between air flow rate and pressure amplitude

increase. But there appear some discrepancies in the outer ranges. This seems to be attributable to the simplification that the ignition lag τ_{ign} has a constant value of 0.02 sec regardless of the air flow rate change as described in the section 5.2. If the value of ignition lag measured at the corresponding air flow rate is used, it may be possible to give exact prediction also for the other ranges of disagreement.

Figure 14 shows the relations between air flow rate and clearly perceived frequency. The theoretical plots express well the tendency in the experimental curves that the frequency in the same order gradually decreases with an increasing air flow rate.

Figure 15 shows the relation between fuel flow rate and pressure amplitude. Similarly in this case, the theoretical results are in agreement with the experimental ones.

In what follows, on the basis of qualitative characteristics of the theoretical analysis, evaluation will be made on the influences of several factors which have been practically hard to measure separately from other factors.

Figure 16 expresses the influence of ignition lag τ_{ign} on pressure fluctuation. According to the time-course of the pressure amplitude theoretically obtained at a smaller ignition lag such as $\tau_{ign} < 0.48$, pressure amplitude decreased gradually at first up to the period equal to approximately 4-times the Helmholtz periodic time, then it decreased again with the progress in calculation. Maximum and minimum amplitudes shown in the figure are obtained from such time-course of pressure

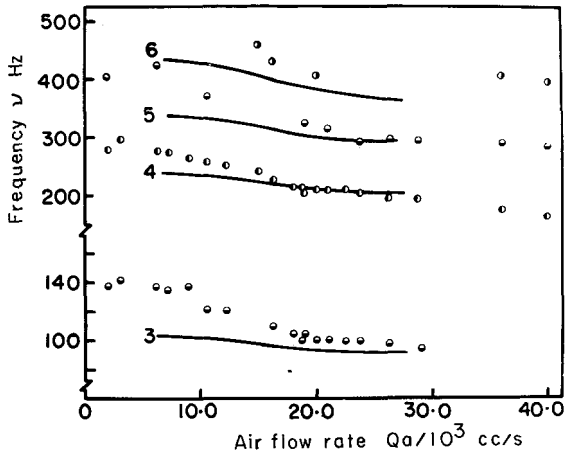

Fig.14 Relations between air flow rate and clearly perceived frequency

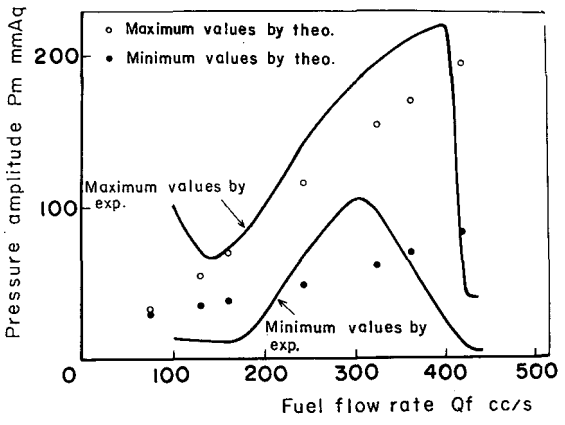

Fig.15 Relations between fuel flow rate and pressure amplitude

amplitude. Especially, the difference between maximum and minimum amplitudes is large at τ_{ign} = 0.02 sec, and small at τ_{ign} = 0.01 sec and 0.05 sec. It has already been mentioned that the variations of pressure amplitude are caused as a result of the interference effect between pressure and entropy mode waves; if the results of this figure are combined with the above-mentioned explanation, it can be said that the interference effect depends in a great degree on the ignition lag. In addition, because the theoretical and experimental results coincide with each other in the relations between fuel flow rate and pressure amplitude, it may be understandable that the ignition lag remains nearly constant in the range of the fuel flow rate change of this figure.

Table 2 shows the effects of wall temperature, of coefficient of pipe friction, and of coefficient of heat transfer on pressure amplitude at three observing points. Pressure amplitude decreases both with an increase in heat transfer coefficient and with an increase in heat loss to wall surface, that is, with a decrease in wall temperature ratio, but its decreasing degree is quite low. By considering that in this report the heat release rate distribution has been estimated from the beginning, the following conclusions are drawn. If the changes in wall temperature ratio and in heat transmission are in such a degree that they scarcely affects heat release rate and combustion efficiency, those changes give little effect on the states of oscillatory combustion.

Assuming the pipe friction by the expression in the table is equivalent to changing the sand diameter as carried out by Nikuradse[10], it can be concluded from the numerical values in this table that such an effect of roughness of pipe inner surface on pressure amplitude is negligibly small.

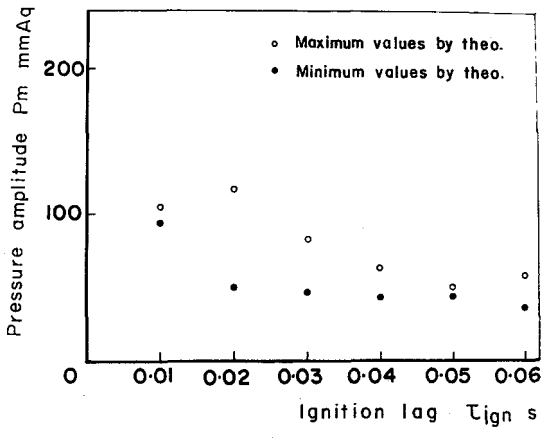

Fig.16 Influence of ignition lag on pressure amplitude

7. Conclusions

Numerical simulation method of non-steady combustion state, especially of oscillatory combustion state is presented. The principal charactristics of the procedurea are summarized as follows :

(1) By integrating numerically

the differential equations for the entropy and pressure modes along each characteristic direction, it has become possible to estimate the intensive heat balance of combustion, and as a result, to obtain detailed knowledge with respect to the changes of state which take place in the combustion systems.

(2) By Fourier transforming the wave forms obtained through numerical calculation for several successive ranges of Helmholtz periodic time, it became feasible to derive the frequency spectrum of and the time-course of pressure amplitude.

The theoretical results were compared with the experimental ones relating to the conditions of the geometrical dimensions of combustion systems and of the fuel and air flow rates. These comparisons revelaed that the calculation procedures are available as a quantitative method for predicting the combustion oscillation phenomena.

Summarization of the results obtained leads to the following conclusions :

(1) Among the clearly observed frequency components, the ones except for the Helmholtz resonant frequency are slightly affected by the volume of air plenum chamber , but are largely influenced by the length of combustion chamber.

(2) It was proved that the pressure amplitude change with time is induced

Tab.2 Relations of effective pressure amplitudes and three variables

Conditions of combustion
Air flow rate 20×10^3 cc/s
Fuel flow rate 243 cc/s

Influence of wall temperature ratio ζ

	P_m mmAq					
	Calc. point a		Calc. point d		Calc. point c	
	max.	min.	max.	min.	max.	min.
0.2	112.72	53.43	41.63	18.56	96.23	44.30
0.4	113.60	51.50	41.15	17.81	96.82	42.61
0.6	115.07	50.37	41.05	17.36	97.92	41.61
0.8	116.64	49.62	41.02	17.02	99.11	40.98

Influence of C_T in the equation of heat transfer

	P_m mmAq					
	Calc. point a		Calc. point d		Calc. point c	
$C_T\times10^5$	max.	min.	max.	min.	max.	min.
6.19	126.89	55.06	44.51	18.85	107.99	45.57
12.38	124.88	53.78	43.82	18.41	106.22	44.49
30.95	116.64	49.62	41.02	17.02	99.11	40.98

Influence of the coefficient of pipe friction
If R_e is greater than $R_{e.limit}$, ξ is estimated by substituting $R_e = R_{e.limit}$ in the equation of $\xi = 0.3164/R_e^{0.25}$

	P_m mmAq					
	Calc. point a		Calc. point d		Calc. point c	
$R_{e.limit}$	max.	min.	max.	min.	max.	min.
3000	117.61	49.90	41.28	17.16	101.17	41.65
9000	117.61	49.90	41.28	17.16	101.17	41.65
27000	117.60	50.06	41.29	17.21	101.15	41.80
71000	117.60	50.29	41.35	17.27	101.08	42.00
∞	116.64	49.62	41.02	17.02	99.11	40.98

by the interference effects between entropy and pressure modes, and that this interaction depends mainly on the ignition lag.

Furthermore, on the basis of the quantitative characteristics of the analytical procedure, examination was carried out with respect to the effects of several factors which were difficult to measure separately from other factors. It is concluded from this examination that the influences of wall temperature ratio and of heat transfer on the pressure amplitude are usually slight and that the effect of the magnitude of pipe friction on the pressure amplitude is little.

References

(1) Streeter, V.L. and Wylie, E.B., *Hydraulic Transients*, (1967), McGraw Hill.

(2) Shapiro, A.H., *The Dynamics and Thermodynamics of Compressible Fluid Flow*, Vol.2 (1957), 930, Ronald Press.

(3) Sauer,R., *Nicht stätionare Probleme der Gasdynamik*,(1966), 89, Springer Verlag.

(4) Yamaguchi,M. and Nogi, T., *Fundamentals of Numerical Analysis* (in Japanese), (1970), 119, Kyoritsu Book Co.

(5) Awano,S. and Uchida, H., *Heat Engines and its Fundamental Theory*, Vol.1, (in Japanese), (1960), 307, Sankaido.

(6) Jenny,E., *The Brown Boveri Review*, 12(1950), 433 and 447.

(7) Shimamoto,Y., Oka, M. and Tanaka, Y., *Bulletin JSME*,21-153(1978-3),502.

(8) Tanaka,Y. and Shimamoto, Y., *Bulletin JSME*,19-138(1976-12), 1530 and 1539.

(9) JSME Edition,*Handbook for Mechanical Engineers, 4th Edit.*, (in Japanese), (1962), JSME.

(10) refer to pages 16 and 17 in Vol.8 of Reference (9).

(11) refer to page 1548 of Reference (8).

(12) Tanaka, Y. and Shimamoto, Y., *Progress on Combustion* (in Japanese), 42 (1976-8),1